

# The fate of mesenchymal stem cells is greatly influenced by the surface chemistry of silica nanoparticles in 3D hydrogel-based culture systems

**Darouie, Sheyda; Ansari Majd, Saeid; Rahimi, Fatemeh; Hashemi, Ehsan; Kabirsalmani, Maryam; Dolatshahi-Pirouz, Alireza; Arpanaei, Ayyoob**

*Published in:*
Materials Science and Engineering C: Materials for Biological Applications

*Link to article, DOI:*
10.1016/j.msec.2019.110259

*Publication date:*
2020

*Document Version*
Peer reviewed version

# Journal Pre-proof

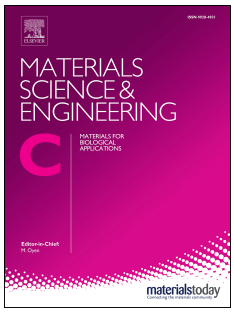


The fate of mesenchymal stem cells is greatly influenced by the surface chemistry of silica nanoparticles in 3D hydrogel-based culture systems

Sheyda Darouie, Saeid Ansari Majd, Fatemeh Rahimi, Ehsan Hashemi, Maryam Kabirsalmani, Alireza Dolatshahi-Pirouz, Ayyoob Arpanaei

PII: S0928-4931(19)31622-4

DOI: https://doi.org/10.1016/j.msec.2019.110259

Reference: MSC 110259

To appear in: *Materials Science & Engineering C*

Received Date: 1 May 2019

Revised Date: 18 September 2019

Accepted Date: 25 September 2019

Please cite this article as: S. Darouie, S.A. Majd, F. Rahimi, E. Hashemi, M. Kabirsalmani, A. Dolatshahi-Pirouz, A. Arpanaei, The fate of mesenchymal stem cells is greatly influenced by the surface chemistry of silica nanoparticles in 3D hydrogel-based culture systems, *Materials Science & Engineering C* (2019), doi: https://doi.org/10.1016/j.msec.2019.110259.

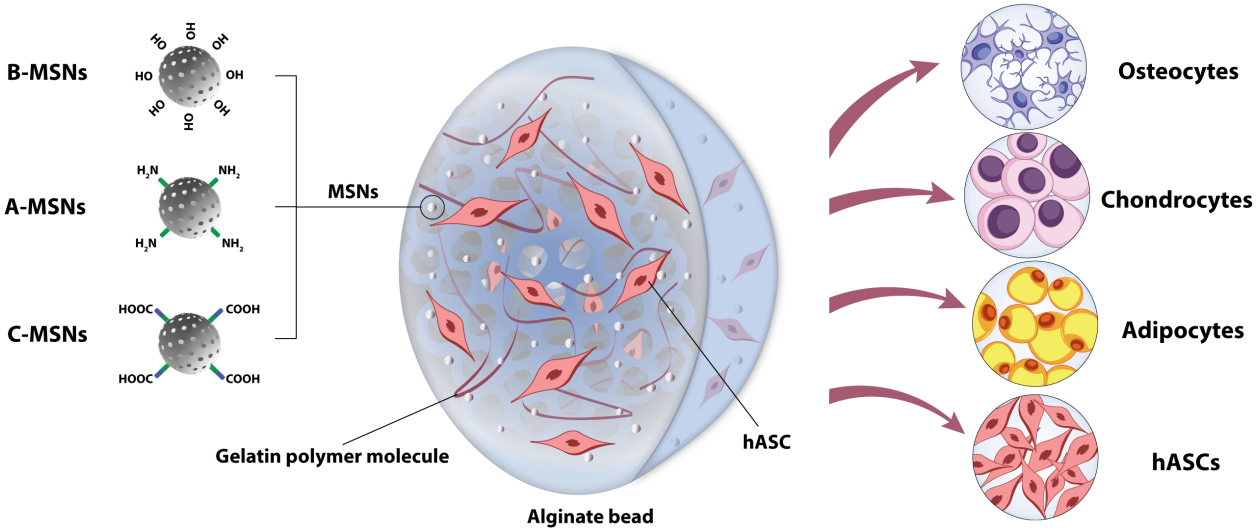

# The fate of mesenchymal stem cells is greatly influenced by the surface chemistry of silica nanoparticles in 3D hydrogel-based culture systems

*Sheyda Darouie[a,b], Saeid Ansari Majd[c], Fatemeh Rahimi[a], Ehsan Hashemi[c], Maryam Kabirsalmani[d], Alireza Dolatshahi-Pirouz[e,f], and Ayyoob Arpanaei[a,]**

AUTHOR ADDRESS

Sheyda Darouie
[a] Department of Industrial and Environmental Biotechnology, National Institute of Genetic Engineering and Biotechnology (NIGEB), P.O. Box: 14965/161, Tehran, Iran.
[b]Department of Health Technology, Technical University of Denmark (DTU), 2800 Kgs, Denmark. Email: sheydarouie@gmail.com

Saeid Ansari Majd
[c] Department of Animal Biotechnology, National Institute of Genetic Engineering and Biotechnology (NIGEB), P.O. Box: 14965/161, Tehran, Iran. Email: s_ansari@nigeb.ac.ir

Fatemeh Rahimi
[a] Department of Industrial and Environmental Biotechnology, National Institute of Genetic Engineering and Biotechnology (NIGEB), P.O. Box: 14965/161, Tehran, Iran. Email: rahimi12@nigeb.ac.ir

Ehsan Hashemi
[c] Department of Animal Biotechnology, National Institute of Genetic Engineering and Biotechnology (NIGEB), P.O. Box: 14965/161, Tehran, Iran. Email: e.hashemy@gmail.com

Maryam Kabirsalmani
[d] Department of Stem Cell and Regenerative Medicine, Faculty of Medical Biotechnology, National Institute of Genetic Engineering and Biotechnology (NIGEB), P.O. Box: 14965/161, Tehran, Iran. Email: kabirs_m@yahoo.com

Alireza Dolatshahi-Pirouz
[e] DTU Nanotech, Center for Intestinal Absorption and Transport of Biopharmaceuticals, Technical University of Denmark (DTU), 2800 Kgs, Denmark.
[f] Department of Regenerative Biomaterials, Radboud University Medical Center, Philips van Leydenlaan 25, Nijmegen 6525 EX, The Netherlands. Email: alirezadolatshahipirouz@gmail.com

*** Corresponding Author**

Ayyoob Arpanaei
[a] Department of Industrial and Environmental Biotechnology, National Institute of Genetic Engineering and Biotechnology (NIGEB), P.O. Box: 14965/161, Tehran, Iran. E-mail: arpanaei@yahoo.com, aa@nigeb.ac.ir, Tel.: +98 2144787463, Fax: +98 2144787395

## Highlights

- Mesoporous silica nanoparticles were used to reinforced polysaccharide-based hydrogels
- Nanoparticles surface chemistry and concentration highly affect stem cells fate and homogeneity in hydrogel-based 3D scaffolds
- Encapsulated human adipose-derived stem cells maintain their stemness when cultured in alginate/gelatin hydrogel beads incorporated with amine-functionalized silica nanoparticles

## Abstract

Polymeric hydrogel-based 3D scaffolds are well-known structures, being used for cultivation and differentiation of stem cells. However, scalable systems that provide a native-like microenvironment with suitable biological and physical properties are still needed. Incorporation of nanomaterials into the polymeric systems is expected to influence the physical properties of the structure but also the stem cells fate. Here, alginate/gelatin hydrogel beads incorporated with mesoporous silica nanoparticles (MSNs) (average diameter 80.9 ± 10 nm) and various surface chemistries were prepared. Human adipose-derived mesenchymal stem cells (hASCs) were subsequently encapsulated into the alginate/gelatin/silica hydrogels. Incorporation of amine- and carboxyl-functionalized MSNs (A-MSNs and C-MSNs) significantly enhances the stability of the hydrogel beads. In addition, the expression levels of *Nanog* and *OCT4* imply that the incorporation of A-MSNs into the alginate/gelatin beads significantly improves the proliferation and the stemness of encapsulated hASCs. Importantly, our findings show that the presence of A-MSNs slightly suppresses *in vivo* inflammation. In contrast, the results of marker gene expression analyses indicate that cultivation of hASCs in alginate beads incorporated with C-MSNs (10% w/w) leads to a heterogeneously differentiated population of the cells, *i.e.,* osteocytes, chondrocytes, and adipocytes, which is not appropriate for both cell culture and differentiation applications.

**Keywords:** Alginate Bead, Gelatin, Mesoporous Silica Nanoparticle, Mesenchymal Stem Cell, 3D Scaffold.

## 1. Introduction

Recently, great attention has been paid to cell therapy and personalized medicine; their clinical applications can hopefully cure various types of diseases in the near future [1–3]. Mesenchymal stem cells (MSCs) have a high potential for medical applications due to their differentiation capabilities into various types of cells [1,2]. However, these cells have a fairly limited cell population and grow slowly; they can also propagate *via* uncontrolled differentiation [3]. Even though there is an urgent need to expand MSCs *in vitro*, the use of continuous passages to reach a high number of cells over a long duration reduces the activity and ability of stem cells to proliferate and differentiate. This phenomenon happens due to phenotypic and genotypic changes while stem cells are being adapted to their surrounding environment [4]. Therefore, a multifunctional synthetic niche similar to the native microenvironment in the human body is needed for the cultivation of homogeneous populations of undifferentiated stem cells. In other words, the situation in which stem cells can sustain their stemness capacity or postpone their differentiation procedure in a controlled manner is missing [5,6].

The ultimate aim of tissue engineering and cell therapy is to mimic the native-like niches in the body; first, to preserve pluripotency properties and genetic stability of stem cells and second to direct cells fate toward the intended destination [7–10]. An appropriate scaffold should have the following traits: (a) provide an adequate level of cell adhesion and migration, (b) provide an appropriate structure for cells, (c) be capable of storing and delivering biomolecules that are essential for cell growth and differentiation, (d) offer enough mechanical stiffness and transfer of mechanical signals, and (e) be eligible for diffusion and mass transferring [11,12]. There have been many attempts to develop new scaffolds for cell culturing, propagation and/or differentiation in recent years but no satisfying solution

yet [13,14]. The challenges that lie ahead of this issue are weaknesses in biocompatibility, bioactivity/biofunctionality, biodegradability, penetrability, mechanical cues, as well as scalability of the system to determine proper cellular fate [11,15,16].

Several approaches have been applied to address these challenges including functionalization of the scaffolds with bioactive molecules [17,18], combination of various types of biomaterials [19,20], incorporation of chemical ions and molecules [21,22] and nanomaterials [23–27], or a combination of these [28,29]. 3D multifunctional scaffolds are increasingly favored because they can mimic the structure of the natural ECM and provide a condition for the spatial organization of cells and enhancing the cell-cell interactions [7,8,13,30–32]. However, the scalability of most of these systems is under serious question. The scalability is an important parameter with respect to the high sensitivity of stem cells to their microenvironment components and chemical and physical properties of the scaffold in culture systems in different scales [33]. There is also a neglected matter in the evaluation of developed 3D scaffolds: A homogenous population of the cultivated or differentiated cells is necessary for clinical applications [34]. In most reports, the homogeneity of cultivated and/or differentiated cells is ignored, and only the cell growth, proliferation, and/or differentiation of the cells into one desired lineage are examined [35–37].

Alginate-based hydrogels have extensively been used for the development of scaffolds for stem cell culture applications because they are injectable with high biocompatibility and can form different shapes [38–41]. Alginate hydrogel beads with sizes in the range of few micrometers to several millimeters are suitable structures to develop a system for 3D culture of stem cells in different scales [42,43]; however, alginate also has some limitations. The cell adhesion and growth are not sufficient in alginate structures, and it also lacks enough mechanical strength [38,39]. We have previously reported that the incorporation of silica nanoparticles into the electrospun polymeric scaffolds can enhance the cell attachment and mechanical stability of polymeric scaffolds [44,45]. What's more, studies have

shown that the mechanical stiffness of nanoengineered collagen-based hydrogels can be significantly enhanced through the addition of modified magnetic nanoparticles [46].

To solve these challenges, we report here a multifunctional scaffold based on alginate/gelatin hydrogel beads incorporated with MSNs. We used alginate beads in combination with gelatin as a bioactive polymer; gelatin is a natural protein derived from collagen hydrolysis and as a major component of various connective tissues, it supposed to provide binding sites in hydrogel for the cells to attach to the structure [47,48]. Moreover, by applying MSNs of various surface chemistries, *i.e.*, unfunctionalized (B-MSNs), aminated (A-MSNs), and carboxylated (C-MSNs) in different concentrations one can tune the properties of the cellular microenvironment in the scaffold and enhance the mechanical properties of the hydrogel structure. The other approach for using nanoparticles in 3D systems is to be used as carrier for different drugs [49], growth factors or differentiation inducers [50].

In this work, in the first step, the nanocomposite beads were prepared, and their physical properties were studied. Then, human adipose-derived mesenchymal stem cells (hASCs) were cultured; and their viability, proliferation, stemness, and differentiation were subsequently studied. Next, *in vivo* experiments were performed to determine the biocompatibility of the as-prepared scaffolds at the implant site. Finally, we elucidated the regulatory effect of nanoparticle concentration and surface charge on hASCs fate.

## 2. Materials and methods

### 2.1 Synthesis, functionalization, and labeling of mesoporous silica nanoparticles

MSNs were synthesized based on a reported approach *via* template removing method [51]. In brief, cetyl trimethylammonium bromide (CTAB) (Sigma-Aldrich, UK) (100 mg) was dissolved in a mixture of deionized (DI) water (48.650 mL) and sodium hydroxide (NaOH) (Sigma-Aldrich, UK) (350 µl, 2 $_M$) with constant stirring (pH of solution ~ 11.7) (solution A). After obtaining a clear solution at 80 °C,

tetraethyl orthosilicate (TEOS) (Sigma-Aldrich, UK) (1 mL) was added drop-wise to solution A (1 $ml.min^{-1}$), and the mixture was stirred for 2 h. In order to remove CTAB, B-MSNs were refluxed in a solution of hydrochloric acid and ethanol with a ratio of 1:10 (v/v). After 12 h, the mixture was centrifuged, and the obtained B-MSNs were washed three times with absolute ethanol (Sigma-Aldrich, UK) and DI water, respectively.

In order to track nanoparticles within hydrogels, fluorescein isothiocyanate (FITC)-labeled MSNs also were fabricated based on the previously mentioned method with some modifications introduced by Rashidi *et al.*[52] Briefly, 3-(2-aminoethyl amino) propyltrimethoxysilane (EDS) (Sigma-Aldrich, UK) (50 µl) was stirred with FITC (Sigma-Aldrich, UK) (0.5 mg) in absolute ethanol (300 µl) in the dark for 2 h (solution B). Then, TEOS (1 ml) was added to solution B and stirred for 5 min (solution C). Next, solution C was added to solution A at 80°C and mixed for 2 h. The subsequent procedure was the same as MSNs synthesis.

To modify the surface of MSNs and FITC-labeled MSNs through the grafting procedure, EDS and succinic anhydride (SA) (Sigma-Aldrich, UK) were used to obtain amine- and carboxyl- functionalized MSNs and FITC-labeled MSNs (A-MSNs/F-A-MSNs and C-MSNs/F-C-MSNs), respectively [53]. Here, B-MSNs/F-B-MSNs (50 mg) was dispersed in absolute ethanol (4.6 ml) followed by addition of DI water (200 µl) for hydrolysis and glacial acetic acid (Sigma-Aldrich, UK) (100 µl) as the catalyst. Then, EDS (100 µl) was added, and the solution was stirred for 1 h at 1000 rpm. Then, A-MSNs/F-A-MSNs was washed three times with ethanol and DI water. The as-prepared A-MSNs/F-A-MSNs was used to achieve C-MSNs/F-C-MSNs. A-MSNs/F-A-MSNs (100 mg) was washed, and this was well dispersed in N,N-dimethylformamide (DMF) (20 mL) (Sigma-Aldrich, UK). Also, SA (200 mg) was dissolved in another batch of DMF (20 mL), and the solution was stirred under a nitrogen atmosphere at 1000 rpm. After 20 minutes, a solution of well-dispersed A-MSNs/F-A-MSNs was added to the

solution of SA in DMF dropwise, and the resulting solution was stirred at room temperature for 24 h. The C-MSNs/F-C-MSNs were washed three times with DMF, ethanol, and DI water, respectively.

### 2.2 Characterization of MSNs and FITC-labeled MSNs

A scanning electron microscope (SEM) (Tescan Vega-3 XMU, Czech Republic) was used to characterize the particle sizes and morphologies. The size distribution of particles (on three different images taken at three different locations) and the average diameter of MSNs was evaluated by ImageJ software, version 1.51n with SEM images. The surface functionalization of MSN samples was evaluated by zeta potential (ζ) measurements of ultrasonicated particles in deionized water using a Malvern Zetasizer Nano ZS (UK). FITC-labeled MSNs were analyzed by Axiophot Zeiss fluorescence microscope (Zeiss, Germany). To determine the specific surface area of the as-prepared MSNs, BET (Brunauer, Emmett, Teller) analysis was applied using a surface area analyzer (Micromeritics TriStar II 3020, USA).

### 2.3 Human adipose-derived mesenchymal stem cell (hASCs) isolation and validation

Collagenase I solution (Sigma-Aldrich, UK) (0.075% (w/v)) in phosphate buffered saline (PBS) containing penicillin-streptomycin (Sigma-Aldrich, UK) (1% w/v) was prepared. Adipose tissue was obtained from human subcutaneous fat harvested by liposuction (from five healthy, female donors with the written permission) and mixed with warm PBS-collagenase I solution at a ratio of 1:1 (v/v). They were then placed in a 37 °C water bath for 1 h. After deactivation of the enzyme by fetal bovine serum (FBS), a well-mixed solution was centrifuged at 300×g for 10 min. The supernatant was then aspirated, and media containing FBS (10%) was added to the cell pellet and resuspended. The hASCs were seeded into T175-$cm^2$ flasks. All cells were cultured at 37 °C in a humidified atmosphere (90%) with 5% $CO_2$.

Before using the cells for experimental tests, hASCs at passage 3-4 were validated by immunophenotyping and differentiation procedures. They were first analyzed by BD FACS Calibur flow cytometer (BD biosciences, San Jose, USA). Specific antibodies of mouse anti-human mesenchymal stem cells including CD90-FITC, CD105-PE, CD73-PE (Exbio, Czech Republic), and CD44-FITC (Immunostep, Spain); hematopoietic stem cell markers included CD45-FITC (BD Biosciences, San Jose, USA) and CD34-PE (Exbio, Czech Republic). The multipotency capability of these cells was then validated by their differentiation induction into osteocytes and adipocytes. To confirm differentiation, real-time PCR and alizarin red (Sigma-Aldrich, UK) and oil red (Sigma-Aldrich, UK) staining methods were used for osteogenic and adipogenic differentiation, respectively.

The multipotency of the hASCs was validated by differentiation to osteogenic and adipogenic lineages. For osteogenic differentiation, cells were seeded at 15000 cells.cm$^{-2}$ by adding osteogenic medium containing FBS (10%), β-glycerophosphate (Sigma-Aldrich, UK), dexamethasone (Sigma-Aldrich, UK), and L-ascorbic acid-2-phosphate (Sigma-Aldrich, UK). The medium was changed every 3–4 days. After 21 days, the cells were washed with PBS and then fixed for 10 min with glutaraldehyde (Sigma-Aldrich, USA) (2.5%) and rinsed with PBS. Mineralization was observed by staining and 10 min of incubation with alizarin red. For adipogenic differentiation, cells were seeded at 15,000 cells.cm$^{-2}$ with adipogenic medium containing FBS (10%), insulin, 1-methyl-3 isobutylxanthine (Sigma-Aldrich, UK), dexamethasone (Sigma-Aldrich, UK), and indomethacin (Sigma-Aldrich, UK). The medium was changed every 3–4 days. After 21 days, the cells were washed with PBS and then fixed for 10 min with glutaraldehyde (2.5%) and washed again with PBS. To observe lipid droplets, the cells were incubated for another 10 min with oil red and washed with PBS. Finally, all samples were visualized using bright-field microscopy (Axiophot Zeiss, Germany).

**2.4 Preparation and characteristics of alginate/gelatin beads**

The solution of a high mannuronic acid (M) content sodium alginate (mannuronic/guluronic acid (M/G) ratio of 1.56) (100 µl, 1% w/v) with and without a fixed concentration of gelatin (0.2% w/v) was dissolved in culture media (DMEM-F12). At the same time, the sample was mixed with $5\times10^4$ human adipose-derived stem cells (hASCs).$ml^{-1}$. Various concentrations of functionalized MSNs (0, 2, 5, and 10%) were loaded into a 31-gauge insulin syringe type and extruded through a needle in a dropwise manner in the $CaCl_2$ solution (0.1 $_M$) while being stirred. The calcium alginate beads are formed due to the crosslinking phenomenon. For the decomposition of alginate/gelatin/MSN beads, sodium citrate solution (0.1 $_M$) in PBS was used along with shaking at 120 rpm for 10 min.

To validate the successful internalization of the gelatin in gelatin/alginate beads, FTIR spectra of the freeze-dried samples were recorded using Fourier transform infrared (ATR-FTIR) spectroscopy (PerkinElmer Spectrum 100 FTIR spectrometer, USA). To evaluate the physical properties of the hydrogel beads, the stability of the alginate/gelatin beads with and without nanoparticles was evaluated by shaking at 80 rpm in terms of the percentage of intact beads remaining on days 1, 3, 7, 14 and 21. Moreover, the swelling profile of the hydrogels in water were determined after 12, 24, 36, 48 and 72h.

The dispersion of MSNs within alginate and alginate/gelatin beads was performed using different concentrations of F-B-MSNs, F-A-MSNs, and F-C-MSNs at various concentrations.

**2.5 Cell proliferation and In vitro biocompatibility studies of hydrogel beads**

To measure the total number of cells, the isolated cells from decomposed hydrogels on days 1, 3, 7, and 14 were counted by a hemocytometer using bright-field microscopy. The cell numbers at day 0 were counted to evaluate encapsulation efficiency (Fig. S1). *In vitro* biocompatibility of the as-prepared MSNs with and without hydrogel beads was evaluated by optical density (OD) measurements of formazan crystals at 580 nm. The tests include 2D and 3D (3-(4,5-dimethylthiazol-2-yl-2,5-diphenyl tetrazolium bromide) (MTT) (Sigma-Aldrich, UK) assay and fluorescein diacetate/propidium iodide (FDA/PI) (Sigma-Aldrich, UK) staining within the hydrogels. For 2D experiments, hASCs were

suspended in DMEM-F12 and then seeded in 96-well plates (10000 cells per well). For 3D experiments, hASCs encapsulated within alginate beads at the days 1, 3, 7 and 14 were removed from their culture media and placed in new 24-well plates. The MTT solution was mixed with DMEM-F12 to a final concentration of 0.5 $mg.mL^{-1}$. This solution (200 µL) was then added to each well plate in both 2D and 3D conditions and incubated for 4 h at 37°C. During this time, the cells took up the MTT, and it reduced to insoluble blue formazan crystals. Then, dimethyl sulfoxide (DMSO) (500 µL) (Sigma-Aldrich, UK) was added to each well and incubated at room temperature and shaken for 10 min; each sample (100 µL) was placed in a new 96 well plate, and the OD was measured at 580 nm. A fluorescence-based live/dead assay was performed with FDA/PI staining. FDA (with the final concentration of 8 $\mu g.ml^{-1}$) and PI (with the final concentration of 100 $\mu g.ml^{-1}$) were mixed with FBS-free media (5 ml). After removing the cell culture media, the staining solution was added to the well plates containing alginate beads encapsulated hASCs. The staining solution was removed after 5 min of incubation at room temperature, and the hydrogel beads were washed twice with PBS. Analysis with fluorescent microscopy (Axiophot Zeiss, Germany) used to calculate the percentages of green nuclei (live cells) and red nuclei (dead cells). The total number of cells were obtained from the sum of all nuclei counted within the gel, and the percentages of cell viability were calculated as follows:

$$\text{Viability } (\%) = \frac{\text{Live cells}}{\text{Total cells}} \times 100 \qquad (1)$$

**2.6 In vivo subcutaneous implantation of hydrogel beads**

In this experiment, 12 albino Wistar rats (aged ~12 weeks) were kept under standard laboratory conditions at 20 ± 2 °C on a 12:12 h light/dark cycle with access to water and food. All animal procedures were done based on the guideline of the American Veterinary Medical Association (AVMA). Before the test, animals were anesthetized by ketamine/xylazine (100/12.5 $mg.kg^{-1}$). The fur on the dorsal area was then shaved. Sterile hydrogels were implanted subcutaneously (placed between

skin and fascia). Finally, animals were closed and received topical tetracycline and followed-up for 3 weeks post-implantation.

The rats were sacrificed four weeks after implantation, and the desired tissues (liver, spleen and implanted site) were isolated to analyze any pathological changes *via* hematoxylin and eosin (H&E) and immunohistochemistry tests. The samples were paraffin-embedded following fixing in 10% formaldehyde. The samples underwent H&E staining; the prepared tissue samples were evaluated by light microscope. Any immune reactions were evaluated using immunohistochemistry to detect the expression of CD3 and CD68 proteins. Finally, the intensity of fluorescence was evaluated using ImageJ software.

### 2.7 Real-time PCR analysis to evaluate stemness capacity and differentiation of hASCs

Real-time PCR for the marker genes *Nanog* and *OCT4* were performed to evaluate the stemness capacity of cultivated hASCs before and after the encapsulation. The desired differentiation gene markers for osteogenic (*RUNX2* and *OC*), adipogenic (*AP2* and *FABP4*), and chondrogenic (*ACAN* and *COLX*) differentiations were utilized (Table S2). For RNA isolation of hASCs cultivated in 2D culture plates, $10^6$ cells were pelleted, dissolved in 1 mL TRIzol Reagent (Invitrogen, Life Technology, USA), and stored at −70°C until use. In 3D experiments, to obtain single cells, the alginate/gelatin/silica beads were decomposed *via* a sodium citrate solution. Those cells were then treated like 2D cultured cells. RNA was isolated following the TRIzol protocol. The total RNA was quantified using NanoDrop ND-1000 Spectrophotometer (Nanodrop Technologies). In cDNA synthesis, RNA (1000 ng) was utilized as a template using a cDNA synthesis kit (Thermo Scientific, USA). The target genes (primers are listed in Table S2) were normalized to the reference housekeeping *GAPDH* gene according to the $2^{-\Delta\Delta Ct}$ method [54].

### 2.8 Statistical Analysis

All continuous variables are represented as the mean ± standard deviation (SD) (n = 3 or 4). Tukey's statistical analysis was performed using one-way analysis of variance (ANOVA). All statistical analyses were performed with GraphPad Prism 6 Software. The statistical significance was displayed as *$p < 0.05$, **$p < 0.01$, ***$p < 0.001$.

# 3. Results and Discussion

## 3.1 Characterization of MSNs and FITC-labelled MSNs

Unfunctionalized and functionalized MSNs and FITC-labeled MSNs were synthesized and characterized. A schematic representation of the synthesis and functionalization methods can be seen in Fig. 1a. The spherical morphology and the average diameter of the as-prepared MSNs (80.9 ± 10 nm) and FITC-labeled MSNs (107.94 ± 15.1 nm) were examined using SEM (Fig. 1b-e). The surface functionalization of MSNs samples was successfully studied *via* zeta potential measurements of the as-prepared nanoparticles: -16, +35 and -25 mV for unfunctionalized MSNs, A-MSNs, and C-MSNs, respectively (Fig. 1f). In addition, zeta potential analysis of variously functionalized FITC-labeled MSNs (*i.e.*, F-B-MSNs, F-A-MSNs, and F-C-MSNs) also imply the successful functionalization of nanoparticles (Fig. 1f).

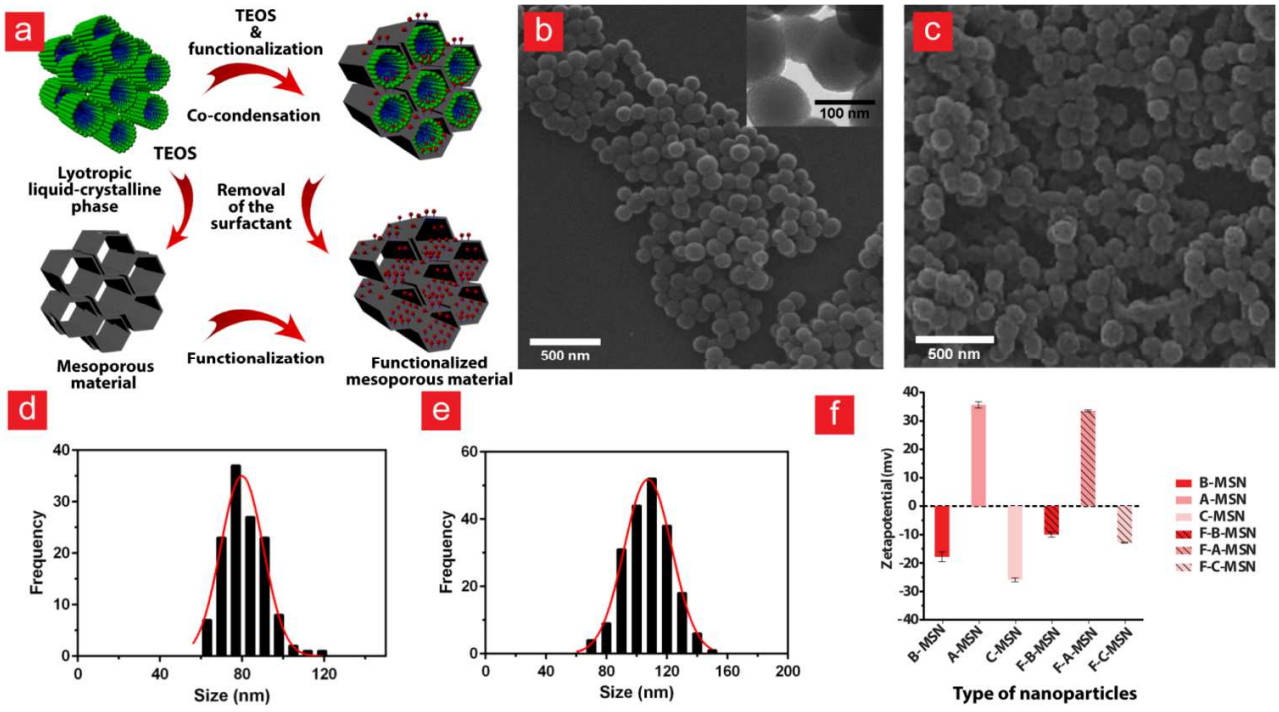


**Fig. 1.** Schematic illustration of MSNs functionalization methods (a). SEM and TEM images of B-MSNs (b) and SEM image of F-B-MSNs (c). Size distribution of B-MSNs (d) and F-B-MSNs (e). Zeta potential values of different MSNs and FITC-labeled MSNs (f). [2-column image-preference for color: online only]

### 3.2 Study of the distribution of FITC-labeled MSNs incorporated into the alginate beads

When adding nanomaterials into hydrogels, a key challenge is avoiding their non-homogenous dispersion within the hydrogel matrix [55]. The heterogeneous dispersion of nanoparticles within the hydrogel matrix might lead to large variations in the cells' responses and fates. Thus, a study of the dispersion homogeneity of MSNs within alginate and alginate/gelatin beads was performed using the FITC-labeled nanoparticles in various concentrations. The results indicated a rather homogeneous dispersion of nanoparticles within the hydrogel beads for all types of nanoparticles in various concentrations (Fig. 2). Different color intensities of samples can imply different values of

nanoparticles incorporated into the hydrogel beads (compared to control without nanoparticles, see Fig. S2).

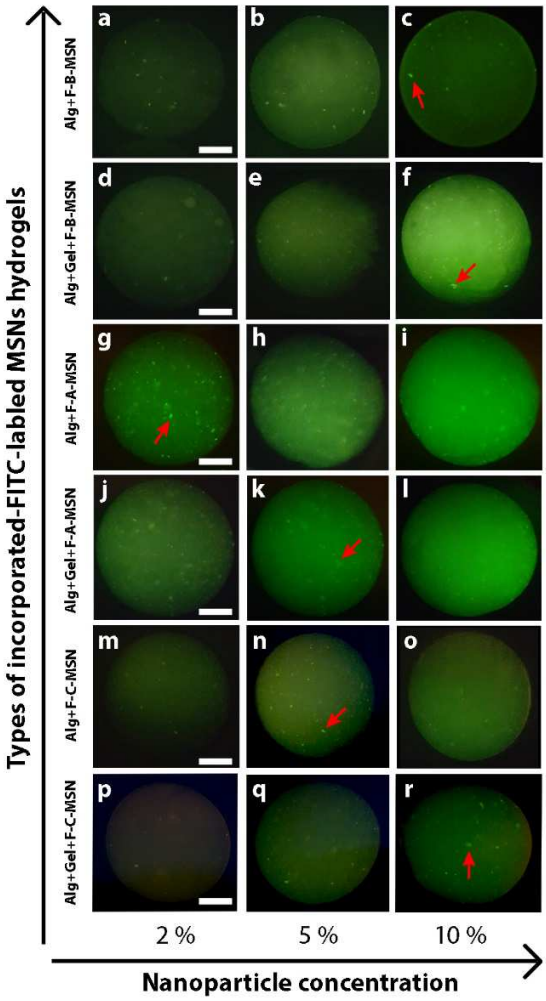


**Fig. 2.** Fluorescent microscopy images of alginate beads incorporated with FITC-labeled MSNs illustrating nanoparticles dispersion in the hydrogel matrix. Alginate beads (Alg) containing different concentrations (2-10% w/w) of F-B-MSNs without (a-c) and with gelatin (Gel) (d-f); F-A-MSNs without (g-i) and with gelatin (j-l), and F-C-MSNs without (m-o) and with gelatin (p-r). Red arrows indicate MSN aggregations, scale bars, 200 µm. [single-column image-preference for color: online only]

### 3.3 Physical properties of MSNs-incorporated hydrogel beads

In preliminary tests, alginate beads were prepared in the presence of various amounts of gelatin values (the mass ratio of gelatin to alginate was from 1:10 to 1:1). The addition of gelatin to the alginate hydrogels at mass ratios over 1:5 prevents gel formation (data not shown). Therefore, the gelatin to alginate mass ratio of 1:5 was chosen for the preparation of all samples containing gelatin.

The size of the as-prepared beads measured with light microscopy was 1-1.5 mm (Table S1). Spherical alginate beads in this size range have considerably higher biocompatibility properties and can better suppress fibrosis in comparison to smaller sizes [56]. The results also indicate that the addition of gelatin decreases the size of the synthesized alginate beads; the incorporation of B- and A-MSNs does not significantly change the size of beads. Interestingly, the addition of C-MSNs into alginate beads considerably increases their size possibly due to their superior hydration properties by carboxylic groups in the structure of these nanoparticles (Table S1). More, the swelling profile (Fig. S3) of the samples shows that beads contained A-MSNs presented higher swelling property compared to those that have C-MSNs and B-MSNs. This means that, probably, A-MSNs induces $Ca^{2+}$ release from the structure. The presence of positively charges nanoparticles enhanced the swelling property. On the other side, the presence of negatively charged nanoparticles could keep $Ca^{2+}$ ions in the structure for a longer time.

Bead stability was studied by counting the number of intact beads after being shaken at 80 rpm for 1-14 days. The results showed that the addition of gelatin causes a significant decrease in the stability of the as-prepared hydrogel beads. Bead structure was monitored by light microscopy and indicated that gelatin partly exits the bead structure during the incubation as suggested by the appearance of cavities in alginate/gelatin beads over a few days of incubation (Fig. S4). This can explain the low stability of alginate/gelatin beads in comparison to the alginate beads. Surprisingly, these cavities were not observed for the MSNs-incorporated alginate/gelatin beads (Fig. S4). Interestingly, the stability was significantly enhanced for beads incorporated with MSNs regardless of the type of MSN surface

chemistry (Fig. 3 and Fig. S5). This observation indicates that nanoparticles within the hydrogel matrix structure can significantly increase its mechanical stability. Furthermore, the addition of functionalized silica nanoparticles, *i.e.*, A-MSNs and C-MSNs, into alginate beads can improve their mechanical stability. Indeed, lower nanoparticle concentrations were sufficient versus those that incorporated with unfunctionalized MSNs, *i.e.*, B-MSNs (Fig. 3 and Fig. S5). These observations indicate that interactions between functional groups of polymers and those on the surface of nanoparticles can play a significant role in the physical stability of beads. Thus, lower concentrations of functionalized MSNs are sufficient to increase the physical stability. The results also demonstrate that hASCs-encapsulated alginate/gelatin beads have lower stability than bare beads (Fig. 3 and Fig. S6). This observation can be attributed to the cell growth and propagation; which in turn can disrupt the hydrogel matrix.

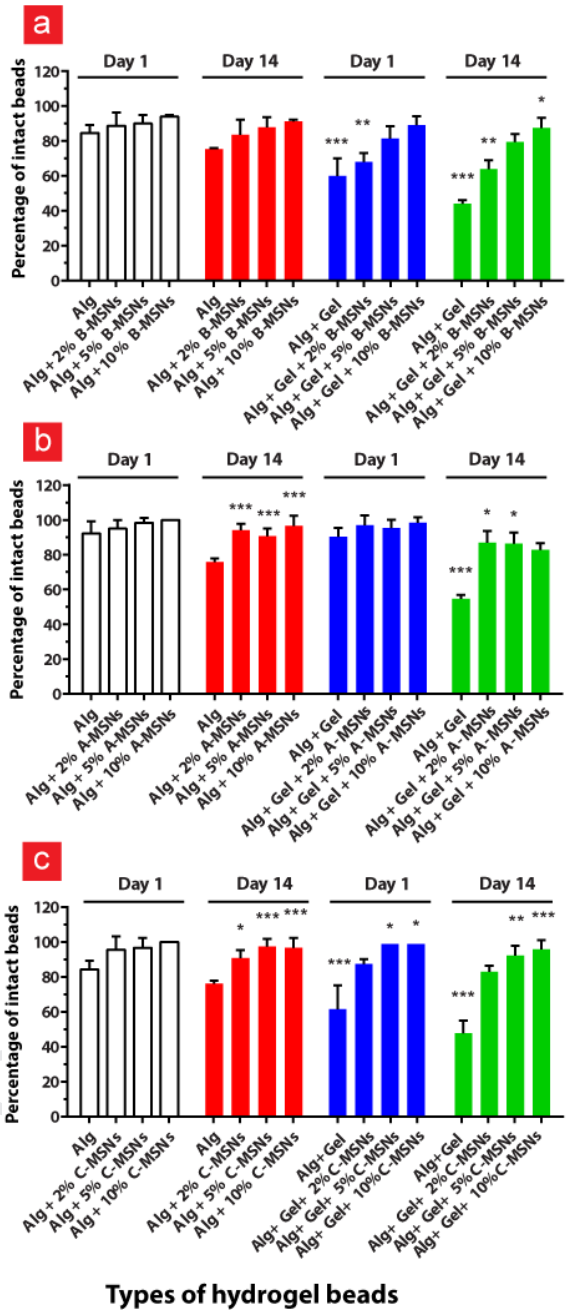


**Fig. 3**. Evaluation of physical stability of hACSs-encapsulated hydrogel beads incorporated with various amounts B-MSNs (a), A-MSNs (b), and C-MSNs (c) in the absence and presence of gelatin (n=4, data compared to Alg as the control for the statistical analysis; *$p < 0.05$, **$p < 0.01$, ***$p < 0.001$). [single-column image-preference for color: online only]

In general, these results indicated that B-MSN-containing beads (10% w/w), A-MSN-containing beads (2% and 5 % w/w), and C-MSN-containing beads (2%, 5% and 10% w/w) all had desired stabilities. Next, samples containing 2% w/w of A-MSNs and C-MSNs and 10% w/w of B-MSNs and C-MSNs were chosen for further investigation.

### 3.4 Study of hASCs proliferation

Before encapsulation, some preliminary tests were conducted to validate the stemness capacity of the isolated hASCs as mesenchymal stem cells. The expression of the cluster of differentiation (CD) markers and differentiation potentials of hASCs to two different lineages (osteocytes and adipocytes) implied the successful isolation of mesenchymal stem cells isolated from fat tissue (Fig. S7).

Nanomaterials can cause some adverse effects on cell growth. Direct counting of the number of total cells revealed that incorporation of A-MSNs into alginate beads does not lead to any significant decrease in the number of viable cells after 14 days (Fig. 4). Interestingly, there was a considerable increase in the number of viable cells when A-MSNs were incorporated into the alginate/gelatin beads. The addition of gelatin can enhance cellular attachments to the scaffold and weaken the attractive interactions between gelatin and alginate molecules and thus lead to leakage of gelatin. This, in turn, can lead to the formation of cavities within the bare beads as stated above (Fig. S4). To overcome this challenge, the gelatin can be covalently cross-linked to the scaffolds [57]; however, cross-linking can lead to cytotoxicity effects and further difficulties [58]. The results suggest that stabilized gelatin along with A-MSNs can strikingly support cell proliferation (Fig. 4). Furthermore, the presence of A-MSNs in the gelatin-free samples shows a better impact on cell propagation versus alginate beads incorporated with negatively charged MSNs, *i.e.*, B- and C-MSNs. This can be attributed to the supportive effect of positively-charged groups of the A-MSNs on enhancing the cell attachment and growth in scaffolds as shown previously in the literature [59].

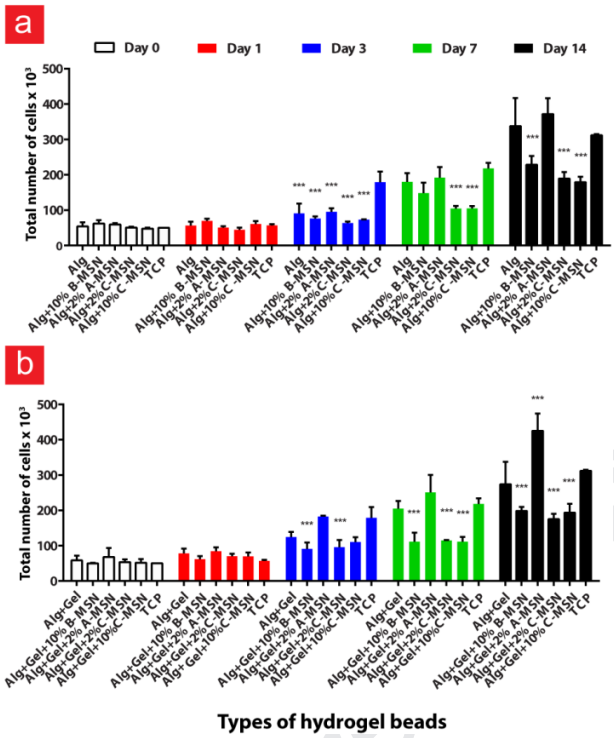


**Fig. 4.** The growth of the hASCs encapsulated within different types of beads measured by direct counting of the number of cells at days 0, 1, 3, 7 and 14. Cell proliferation in nanoengineered alginate beads without (a) and with (b) gelatin (n=3, data compared to tissue culture plate (TCP) as the control for the statistical analysis; ****p<0.001*). [single-column image-preference for color: online only]

### 3.5 Evaluation of the biocompatibility of nanoengineered hydrogel beads

The MTT assay data revealed that applying different concentrations of unfunctionalized and functionalized MSNs does not cause any significant effects on the viability of the cells even at high concentrations tested in a 2D culture condition (Fig. S8). Next, the viability of hASCs encapsulated in nanoengineered hydrogel beads containing various amounts of MSNs (0-10% w/w) was also studied. The results presented in Fig. 5a,b show no significant effect when A-MSNs are added to the hydrogel beads; the addition of negatively charged MSNs, *i.e.*, B- and C-MSNs, shows remarkable adverse effects on proliferation. The cytotoxicity effects of negatively charged nanoparticles and surfaces have been shown in previously published researches [59,60].

In another study, the cell viability was investigated using FDA/PI staining method in 14 days (Fig. 5c,d and Fig. S9). The results confirm the MTT data and show the low cytotoxicity effects of A-MSNs on the cultured cells encapsulated in hydrogel beads.

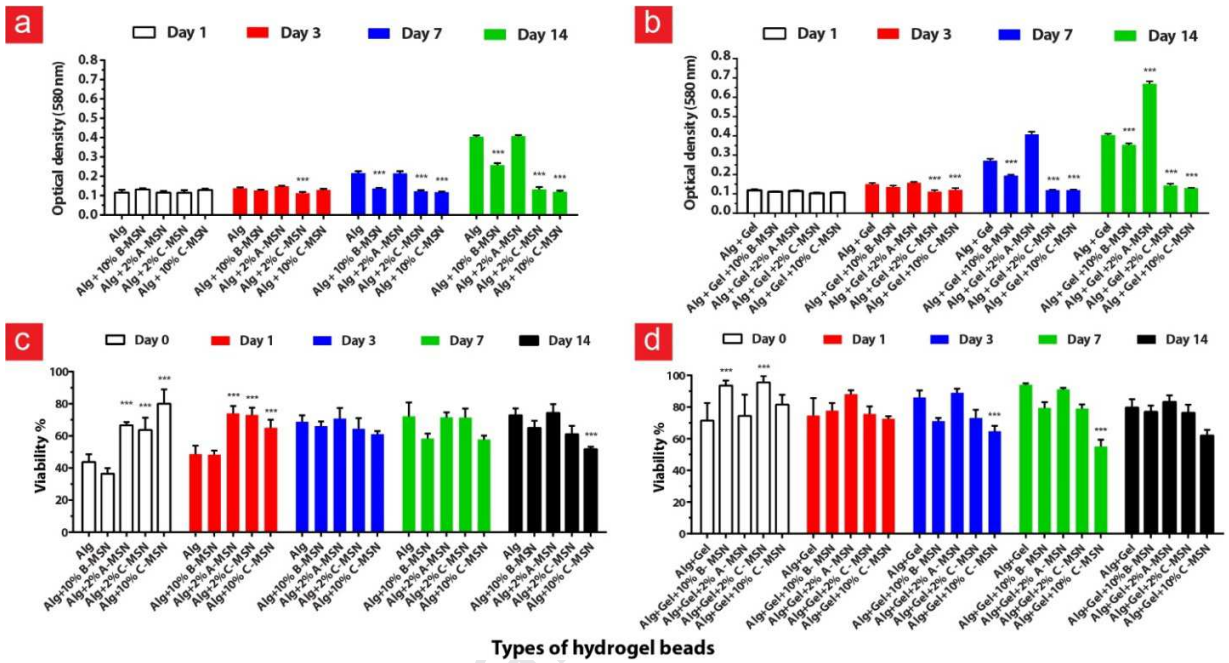


**Fig. 5.** Cytotoxicity effects of different types and concentrations of MSNs for 3D cultured hASCs in alginate beads without (a and c) and with (b and d) gelatin evaluated by MTT assay (a and b) (n=4, data compared with day 1 as a control for the statistical analysis) and live/dead assay by FDA/PI staining (c and d) (n=4, data compared to Alg as a control for the statistical analysis, ****p<0.001*). [2-column image-preference for color: online only]

To investigate the potential of the as-prepared structures for clinical applications, the *in vivo* biocompatibility of the cell-free hydrogels was studied *via* subcutaneous implantation. The initial observation of adverse effects was performed on each animal over the first 30 minutes during the first 4 hours and then up to 21 days. No death or adverse effects were detected in animals during dosing and observation. Next, the host tissue-specific response to implantation of hydrogels was followed for 3 weeks. Fig. 6a shows the process of subcutaneous implantation of the hydrogel beads into the host

tissue. There were no side effects after three weeks for the embedded hydrogel beads in the tissue, and the tissues adjacent to the hydrogel beads looked normal (Fig. 6b).

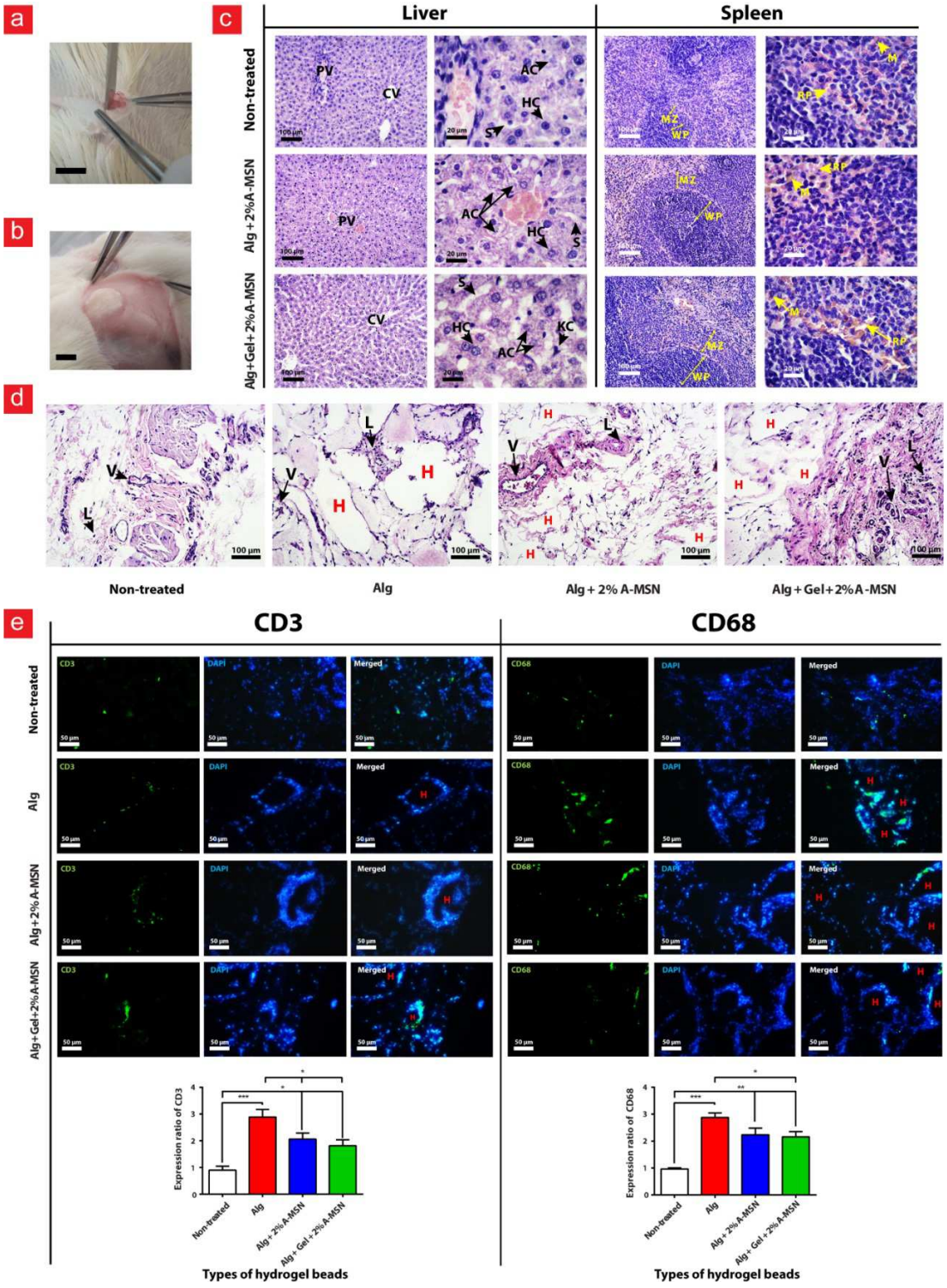


**Fig. 6.** Pathological studies of tissues implanted with nanoengineered hydrogel beads. The process of subcutaneous hydrogel bead implantation (scale bar, 1 mm) (a). Embedded hydrogels into rat omentum/fat tissue

after 21 days (scale bar, 1 mm) (b). H&E stained histological sections of liver and spleen at day 21; PV: portal vein, CV: central vein, AC: apoptotic cell, HC: hepatocyte, S: sinusoid, KC: Kupffer cell, MZ: marginal zone, WP: white pulp, M: macrophage, RP: red pulp (c). H&E stained histological sections of implanted regions at day 21 showed no signs of inflammation in the adjacent tissues; V: vein, L: lymphocyte, H: hydrogel (d). Immunohistochemistry analysis for CD3 and CD68 inflammatory markers and their related expression rate in implanted sites at day 21 quantified using ImageJ; CD68 and CD3 (in green), nuclei (DAPI, in blue), H: hydrogel (e). (n=3 rats per treatment and H&E and immunohistochemistry sections, *$p < 0.05$, **$p < 0.01$, ***$p < 0.001$). [2-column image-preference for color: online only]

In Fig. 6c, H&E staining results imply a normal architecture of liver (normal hepatocytes, Kupffer cells, and veins) seen in response to the hydrogel implantation as compared to the non-treated group. Although the architecture of the liver seems normal, the images for the hydrogel-injected groups (both Alg+2%A-MSNs and Alg+Gel+2%A-MSNs) indicate a slightly higher number of apoptotic cells in comparison to that of the non-treated group (Fig. 6c). This response was expected since the liver acts as a detoxification tissue and filters toxins. Therefore, cell apoptosis might occur more as a side effect of hydrogel injection and/or degradation.

In spleen sections, both Alg+2%A-MSNs and Alg+Gel+2%A-MSNs samples showed a normal architecture with normal lymphoid follicles and well defined red and white pulps versus the non-treated group. However, some pathological changes such as red and white pulps had been widened but had not congestion or any other damage observed (Fig. 6c).

The embedding of hydrogels into host tissue was further confirmed by H&E images including the formation of numerous blood vessels at the tissue-hydrogel interface site (implantation site). Furthermore, lymphocytes were obviously seen in the sections, and these are evidence for blood cell formation in implantation sites. These results represent implanted hydrogels as histocompatible biomaterial (Fig. 6d).

Moreover, to evaluate the possible inflammatory response to the implanted hydrogels, expression of CD3 (a T-lymphocyte marker), and CD68 (a protein expressed by macrophages and monocytes) were measured at implant sites. Overall, alginate implants significantly increase the expression of CD3 versus the non-treated group (Fig. 6e) implying a significant inflammatory response to this implant. However, the expression of CD3 implies that the inflammatory responses to the alginate implants considerably decrease in the presence A-MSNs (2% w/w) in contrast to gelatin that does not show any significant effect on the response of the immune system ($P<0.05$) (Fig. 6e).

The expression pattern for CD68 was very similar to that of the CD3. Alginate implants boost CD68 expression, but alginate in combination with A-MSNs considerably ($P<0.05$) lowers the immune responses. These results showed that while hydrogel implants can trigger the immune response in the implant site (as a normal reaction to foreign substances in the body), these reactions can be minimized by incorporating biocompatible A-MSNs into the hydrogels.

### 3.6 Study of stemness capacity of encapsulated hASCs

Expression of pluripotency genes such as *OCT4* and *NANOG* indicates the level of mesenchymal stem cell stemness [61]. The results from real-time PCR show that the stemness of hASCs are maintained when low concentrations (2% w/w) of A- and C-MSNs are used within 14 days of incubation. Moreover, adding gelatin to the structure enhanced the stemness capacity as indicated by higher values of expression of *OCT4* and *NANOG* in comparison to beads without gelatin—especially for alginate beads incorporated with A-MSNs (2% w/w) (Fig. 7). *OCT4* and *NANOG* are two genes that show the cell's proliferation and undifferentiated state. These findings are consistent with data obtained in other studies that gelatin can support cell proliferation and keeping them in the undifferentiated state due to being a highly bioactive polymer and having anchor points on its surface [47,48].

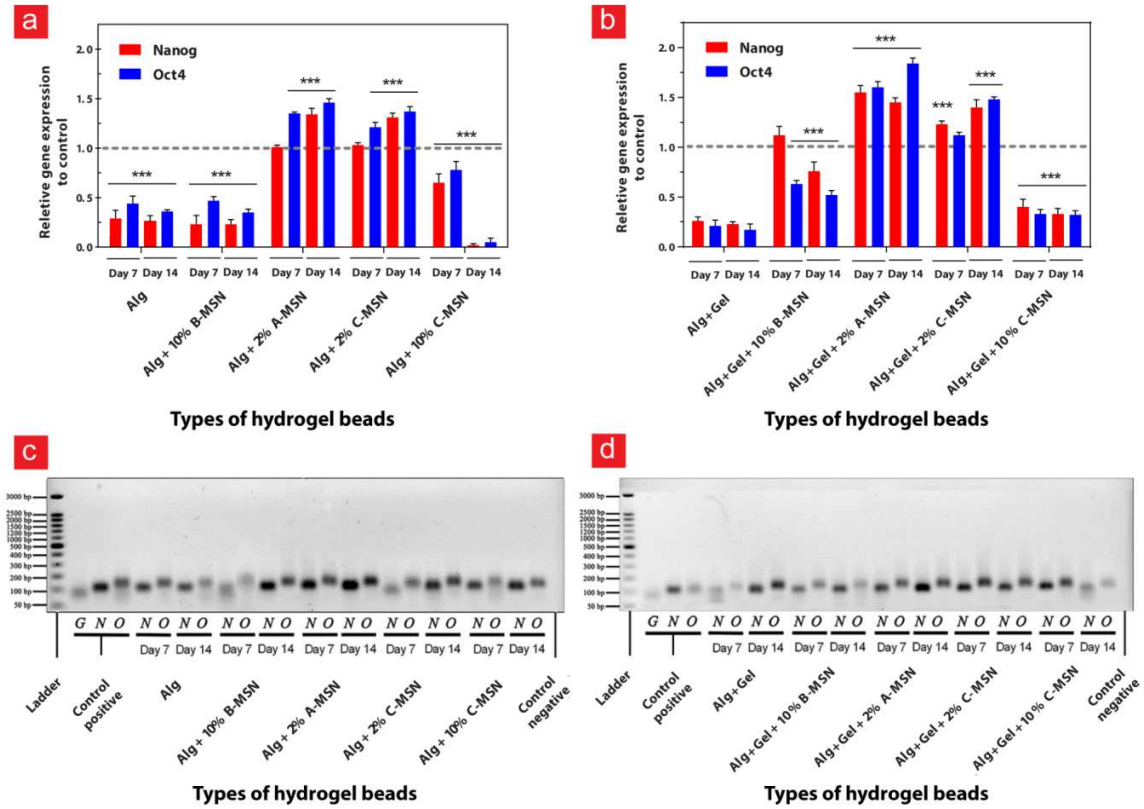


**Fig. 7.** Stemness capacity of cultivated encapsulated hASCs. Real-time analysis to investigate stemness gene expression (N: *NANOG*, O: *OCT4*) of hASCs encapsulated in different types of nanoengineered beads without (a) and with (b) gelatin (n=3, data compared to non-treated sample as a control for the statistical analysis, ****p<0.001*). Gel electrophoresis images of real-time PCR products for samples without (c) and with (d) gelatin. All samples were normalized to the gene expression of 2D-cultivated hASCs. [2-column image-preference for color: online only]

To further investigate the stemness capacity of cultivated hASCs, the expression of various types of differentiation gene markers (*i.e.*, osteogenic, adipogenic and chondrogenic gene markers) was evaluated by real-time PCR (Fig. 8b,c). The lower values of expression of these genes indicate that the cultivated cells in alginate hydrogel beads have not been entirely differentiated and still have retained their stemness capacity. However, after 14 days of culture in 3D structures in the absence of any differentiation factor, the results revealed that different surface chemistries of MSNs have different

effects on the fate of cultivated hASCs. Cells encapsulated in A-MSNs-incorporated beads showed higher stemness capacity and lower differentiation properties indicating a more homogenous cell population in A-MSNs-incorporated hydrogel beads than beads incorporated with negatively-charged MSNs, *i.e.,* B- and C-MSNs (Fig. 8b,c). Furthermore, the addition of gelatin leads to slightly lower

expression of differentiation markers versus those without gelatin.

**Fig. 8.** Study of differentiation capacity of cultivated encapsulated hASCs. A schematic view of the developed nanocomposite system in this work. An alginate bead containing gelatin and MSNs for hASCs culture (a).

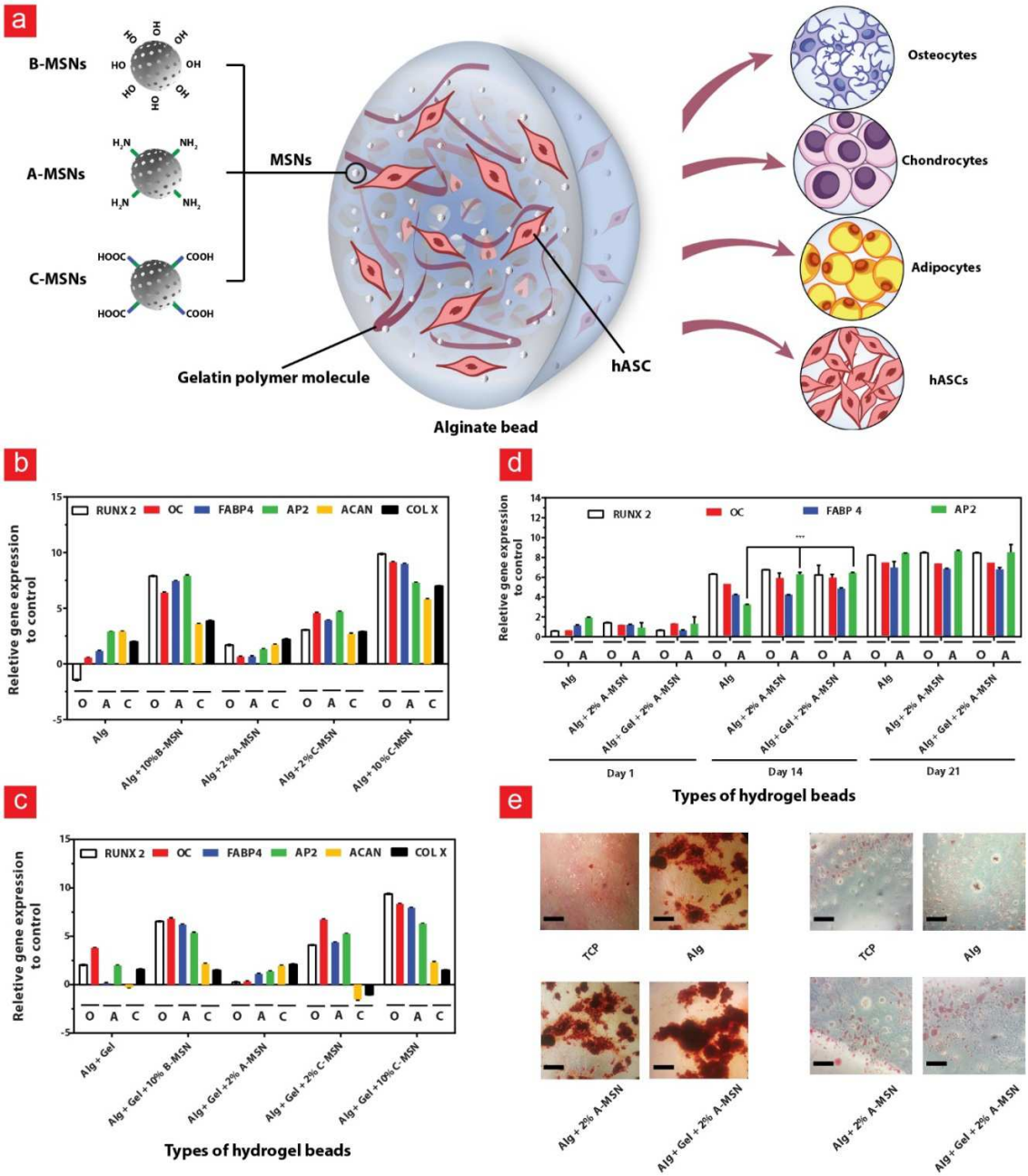


Marker gene expression of osteogenic (O: *RUNX* and *OC*), adipogenic (A: *FABP4* and *AP2*), and chondrogenic

(C: *ACAN* and *COLX*) differentiation were analyzed by real-time PCR for encapsulated cells within alginate beads (b) and alginate/gelatin beads (c). The real-time PCR analysis of marker gene expression of osteogenic and adipogenic differentiation markers after the differentiation induction of re-spread hASCs within alginate and alginate/gelatin hydrogels incorporated with A-MSNs (d) (n=3, data compared to alginate as a control for statistical analysis, ****p<0.001*), scale bar, 200 µm. Induced osteogenic and adipogenic differentiation (e) were further confirmed by alizarin red and oil red, respectively. [2-column image-preference for color: online only]

Fig. 8b,c shows that the hASCs cultivated in C-MSN-incorporated beads are considerably differentiated to osteogenic cells. The C-MSN-incorporated hydrogel beads seem to be a suitable scaffold for osteogenic differentiation of hMSCs in the absence of any differentiation factor. However, the results confirm cell differentiation into adipogenic and chondrogenic lineages (Fig. 8b,c) indicating a heterogeneous population of the cells.

There have been many attempts to direct stem cell differentiation by adjusting cell microenvironment [62–64]. However, studies on the homogeneity of the differentiated cell population is rarely reported. Our findings reveal that high values of expression of a certain differentiation gene marker cannot be sufficient to confirm the performance of the scaffold in the differentiation of stem cells; it is critical to evaluate the homogeneity of the differentiated cell population as well.

As a matter of fact, when stem cells are cultivated in a suitable condition for proliferation, they propagate and retain their stemness capacity. In contrast, the differentiation process is triggered when stem cells are cultivated in a medium that does not support cell proliferation. The different responses of the hASCs to the positively charged MSNs (A-MSNs) and negatively charged MSNs (B- and C-MSNs) can be seen in Fig. 4, 7, and 8a-c, which support this explanation. Over 14 days of culture, the hASCs with higher propagation rates show lower levels of differentiation and *vice versa*. These results agree with the literature in which the physico-chemical properties of the microenvironment affect cell proliferation and differentiation in opposite manners [65,66]. Applying a positively-functionalized

hydrogel increases the osteoblast attachment and proliferation [65] and negatively charged hydrogels induce chondrogenic differentiation [66].

Surprisingly, osteogenic, adipogenic, and chondrogenic gene expressions are highest when 10% C-MSNs are involved in the scaffold versus 2% MSNs of various surface chemistries (Fig. 8b,c). Therefore, the results reveal that both the surface chemistry and concentration of MSNs play key roles in directing stem cell fate and homogeneity. Previously, it has been shown that physical and chemical cues of different types of biomaterials and nanoparticles -specifically MSNs- influenced stem cells fate [67,68]. More, nanoparticles in nanoengineered scaffolds change the physico-chemical properties of the system, which can guide stem cells fate [69].

Next, the differentiation ability of hASCs cultivated in the as-prepared nanoengineered hydrogel beads with the highest values of the stemness capacity was studied using osteogenic and adipogenic differentiation media. The samples were A-MSN-incorporated alginate, A-MSN-incorporated alginate/gelatin, and alginate without MSNs and gelatin as the control. Fig. 8d,e presents the levels of osteogenic and adipogenic differentiation of isolated and re-spread cells cultivated in differentiation media after 21 days of culture. The real-time PCR results and differentiation staining with alizarin red and oil red confirm the high capability of hASCs and their appropriate differentiation levels.

## 4. Conclusions

Nanoengineered alginate/gelatin beads incorporated with mesoporous silica nanoparticles (MSNs) of various surface chemistries were prepared and tested for the human mesenchymal stem cells (hASCs) proliferation/differentiation. The results indicate *in vitro* and *in vivo* biocompatibility of the as-prepared nanoengineered cultivation systems. As expected, the presence of MSNs has a crucial role in the physical stability of the hydrogel beads and stem cell proliferation. Carboxyl-functionalized MSNs (C-MSNs) and amine-functionalized MSNs (A-MSNs) have superior physical stability effects on the hydrogel beads versus bare MSNs (B-MSNs). Surprisingly, the addition of A-MSNs into

alginate/gelatin beads enhances the proliferation performance and leads to considerably higher cell viability and stemness capacity in comparison to that of the alginate beads incorporated with other types of MSNs as well as alginate beads with no MSNs. In addition, a differentiation study of hASCs encapsulated in the as-prepared hydrogel beads revealed a remarkable influence of the MSNs surface chemistry and concentration on the fate of stem cells. In contrast to this situation, the addition of C-MSNs into the hydrogel beads caused the encapsulated hASCs to differentiate into different lineages without any differentiation factors. Hence, having a homogeneous cell population should be a preference for current studies—especially for clinical applications. All in all, the results open up a new window to the field of design and fabrication of scalable multifunctional 3D systems to control stem cells fate. However, comprehensive studies are needed to approve the performance of such systems for clinical applications.

## Acknowledgments

The authors would like to acknowledge the National Institute of Genetic Engineering and Biotechnology (NIGEB) (project number 663), Danish Council for Independent Research (Technology and Production Sciences, 5054–00142B), Gigtforeningen (R139-A3864) and the Villum Foundation (10103) for financially supporting this project. This work is also part of the VIDI research programme with project number R0004387, which is (partly) financed by the Netherlands Organisation for Scientific Research (NWO).

## REFERENCES

[1] J.M. Gimble, A.J. Katz, B.A. Bunnell, Adipose-Derived Stem Cells for Regenerative Medicine, Circ. Res. 100 (2007) 1249–1260. doi:10.1161/01.RES.0000265074.83288.09.

[2] A.I. Caplan, Adult mesenchymal stem cells for tissue engineering versus regenerative medicine, J. Cell. Physiol. 213 (2007) 341–347. doi:10.1002/jcp.21200.

[3] G. Kalamegam, A. Memic, E. Budd, M. Abbas, A. Mobasheri, A Comprehensive Review of Stem Cells for Cartilage Regeneration in Osteoarthritis, in: Adv. Exp. Med. Biol., Springer, New York, NY, 2018: pp. 1–14. doi:10.1007/5584_2018_205.

[4] Y.W. Eom, J.E. Oh, J.I. Lee, S.K. Baik, K.J. Rhee, H.C. Shin, Y.M. Kim, C.M. Ahn, J.H. Kong, H.S. Kim, K.Y. Shim, The role of growth factors in maintenance of stemness in bone marrow-derived mesenchymal stem cells, Biochem. Biophys. Res. Commun. 445 (2014) 16–22. doi:10.1016/j.bbrc.2014.01.084.

[5] N. Chosa, A. Ishisaki, Two novel mechanisms for maintenance of stemness in mesenchymal stem cells: SCRG1/BST1 axis and cell–cell adhesion through N-cadherin, Jpn. Dent. Sci. Rev. 54 (2018) 37–44. doi:10.1016/J.JDSR.2017.10.001.

[6] A. Otte, V. Bucan, K. Reimers, R. Hass, Mesenchymal stem cells maintain long-term in vitro stemness during explant culture., Tissue Eng. Part C. Methods. 19 (2013) 937–48. doi:10.1089/ten.TEC.2013.0007.

[7] C. Lamprecht, M. Taale, I. Paulowicz, H. Westerhaus, C. Grabosch, A. Schuchardt, M. Mecklenburg, M. Böttner, R. Lucius, K. Schulte, R. Adelung, C. Selhuber-Unkel, A Tunable Scaffold of Microtubular Graphite for 3D Cell Growth., ACS Appl. Mater. Interfaces. 8 (2016) 14980–5. doi:10.1021/acsami.6b00778.

[8] P. Zorlutuna, N. Annabi, G. Camci-Unal, M. Nikkhah, J.M. Cha, J.W. Nichol, A. Manbachi, H.

Bae, S. Chen, A. Khademhosseini, Microfabricated biomaterials for engineering 3D tissues, Adv. Mater. 24 (2012) 1782–1804. doi:10.1002/adma.201104631.

[9] P. Bajaj, R.M. Schweller, A. Khademhosseini, J.L. West, R. Bashir, 3D Biofabrication Strategies for Tissue Engineering and Regenerative Medicine, Annu. Rev. Biomed. Eng. 16 (2014) 247–276. doi:10.1146/annurev-bioeng-071813-105155.

[10] A.K. Gaharwar, S. Mukundan, E. Karaca, A. Dolatshahi-Pirouz, A. Patel, K. Rangarajan, S.M. Mihaila, G. Iviglia, H. Zhang, A. Khademhosseini, Nanoclay-enriched poly(ε-caprolactone) electrospun scaffolds for osteogenic differentiation of human mesenchymal stem cells., Tissue Eng. Part A. 20 (2014) 2088–101. doi:10.1089/ten.tea.2013.0281.

[11] D. Barati, S. Ramin, P. Shariati, S. Moeinzadeh, J.M. Melero-martin, A. Khademhosseini, E. Jabbari, Spatiotemporal release of BMP-2 and VEGF enhances osteogenic and vasculogenic differentiation of human mesenchymal stem cells and endothelial colony-forming cells co-encapsulated in a patterned hydrogel, J. Control. Release. 223 (2016) 126–136. doi:10.1016/j.jconrel.2015.12.031.

[12] T. Rozario, D.W. DeSimone, The extracellular matrix in development and morphogenesis: A dynamic view, Dev. Biol. 341 (2010) 126–140. doi:10.1016/J.YDBIO.2009.10.026.

[13] A.K. Gaharwar, A. Arpanaei, T.L. Andresen, A. Dolatshahi-Pirouz, 3D Biomaterial Microarrays for Regenerative Medicine: Current State-of-the-Art, Emerging Directions and Future Trends, Adv. Mater. 28 (2016) 771–781. doi:10.1002/adma.201503918.

[14] M. Mehrali, A.R. Akhiani, S. Talebian, M. Mehrali, S.T. Latibari, A. Dolatshahi-Pirouz, H.S.C. Metselaar, Electrophoretic deposition of calcium silicate–reduced graphene oxide composites on titanium substrate, J. Eur. Ceram. Soc. 36 (2016) 319–332. doi:10.1016/J.JEURCERAMSOC.2015.08.025.

[15] G.M. Harris, T. Shazly, E. Jabbarzadeh, Deciphering the combinatorial roles of geometric, mechanical, and adhesion cues in regulation of cell spreading, PLoS One. 8 (2013) e81113. doi:10.1371/journal.pone.0081113.

[16] Q.L. Loh, C. Choong, Three-Dimensional Scaffolds for Tissue Engineering Applications: Role of Porosity and Pore Size, Tissue Eng. Part B Rev. 19 (2013) 485–502. doi:10.1089/ten.teb.2012.0437.

[17] I. Carmagnola, E. Ranzato, V. Chiono, Scaffold functionalization to support a tissue biocompatibility, in: Funct. 3D Tissue Eng. Scaffolds, Elsevier, 2018: pp. 255–277. doi:10.1016/B978-0-08-100979-6.00011-2.

[18] G.-Y. Du, S.-W. He, C.-X. Sun, L.-D. Mi, Bone Morphogenic Protein-2 (rhBMP2)-Loaded Silk Fibroin Scaffolds to Enhance the Osteoinductivity in Bone Tissue Engineering, Nanoscale Res. Lett. 12 (2017) 573. doi:10.1186/s11671-017-2316-1.

[19] A. Bongso, E.H. Lee, Stem cells: from bench to bedside, World Scientific, 2005. doi:10.1142/5729.

[20] M.H. Murdock, S.F. Badylak, Biomaterials-based in situ tissue engineering, Curr. Opin. Biomed. Eng. 1 (2017) 4–7. doi:10.1016/J.COBME.2017.01.001.

[21] X. Zhang, C. Huang, X. Jin, Influence of K + and Na + ions on the degradation of wet-spun alginate fibers for tissue engineering, J. Appl. Polym. Sci. 134 (2017) 39349–39358. doi:10.1002/app.44396.

[22] S. Bose, S. Tarafder, A. Bandyopadhyay, Effect of Chemistry on Osteogenesis and Angiogenesis Towards Bone Tissue Engineering Using 3D Printed Scaffolds, Ann. Biomed. Eng. 45 (2017) 261–272. doi:10.1007/s10439-016-1646-y.

[23] Y. Lu, M. Li, L. Li, S. Wei, X. Hu, X. Wang, G. Shan, Y. Zhang, H. Xia, Q. Yin, High-activity chitosan/nano hydroxyapatite/zoledronic acid scaffolds for simultaneous tumor inhibition, bone repair and infection eradication, Mater. Sci. Eng. C. 82 (2018) 225–233. doi:10.1016/J.MSEC.2017.08.043.

[24] M. Tanaka, Y. Sato, M. Zhang, H. Haniu, M. Okamoto, K. Aoki, T. Takizawa, K. Yoshida, A. Sobajima, T. Kamanaka, H. Kato, N. Saito, In Vitro and In Vivo Evaluation of a Three-Dimensional Porous Multi-Walled Carbon Nanotube Scaffold for Bone Regeneration, Nanomaterials. 7 (2017) 46. doi:10.3390/nano7020046.

[25] S. Marchesan, L. Ballerini, M. Prato, Nanomaterials for stimulating nerve growth., Science. 356 (2017) 1010–1011. doi:10.1126/science.aan1227.

[26] M. Mehrali, A. Thakur, C.P. Pennisi, S. Talebian, A. Arpanaei, M. Nikkhah, A. Dolatshahi-Pirouz, Nanoreinforced Hydrogels for Tissue Engineering: Biomaterials that are Compatible with Load-Bearing and Electroactive Tissues, Adv. Mater. 29 (2017) 1603612. doi:10.1002/adma.201603612.

[27] K. Huang, J. Wu, Z. Gu, Black Phosphorus Hydrogel Scaffolds Enhance Bone Regeneration via a Sustained Supply of Calcium-Free Phosphorus, ACS Appl. Mater. Interfaces. 11 (2019) 2908–2916. doi:10.1021/acsami.8b21179.

[28] S. Pacelli, F. Acosta, A.R. Chakravarti, S.G. Samanta, J. Whitlow, S. Modaresi, R.P.H. Ahmed, J. Rajasingh, A. Paul, Nanodiamond-based injectable hydrogel for sustained growth factor release: Preparation, characterization and in vitro analysis, Acta Biomater. 58 (2017) 479–491. doi:10.1016/j.actbio.2017.05.026.

[29] T. Jensen, T. Jakobsen, J. Baas, J. V. Nygaard, A. Dolatshahi-Pirouz, M.B. Hovgaard, M. Foss, C. Bünger, F. Besenbacher, K. Søballe, Hydroxyapatite nanoparticles in poly-D,L-lactic acid

coatings on porous titanium implants conducts bone formation, J. Biomed. Mater. Res. Part A. 95A (2010) 665–672. doi:10.1002/jbm.a.32863.

[30] A. Dolatshahi-Pirouz, M. Nikkhah, A.K. Gaharwar, B. Hashmi, E. Guermani, H. Aliabadi, G. Camci-Unal, T. Ferrante, M. Foss, D.E. Ingber, A. Khademhosseini, A combinatorial cell-laden gel microarray for inducing osteogenic differentiation of human mesenchymal stem cells, Sci. Rep. 4 (2015) 3896. doi:10.1038/srep03896.

[31] L. Meli, H.S.C. Barbosa, A.M. Hickey, L. Gasimli, G. Nierode, M.M. Diogo, R.J. Linhardt, J.M.S. Cabral, J.S. Dordick, Three dimensional cellular microarray platform for human neural stem cell differentiation and toxicology, Stem Cell Res. 13 (2014) 36–47. doi:10.1016/j.scr.2014.04.004.

[32] E. Guermani, H. Shaki, S. Mohanty, M. Mehrali, A. Arpanaei, A.K. Gaharwar, A. Dolatshahi-Pirouz, Engineering complex tissue-like microgel arrays for evaluating stem cell differentiation, Sci. Rep. 6 (2016) 30445. doi:10.1038/srep30445.

[33] M. Serra, C. Brito, C. Correia, P.M. Alves, Process engineering of human pluripotent stem cells for clinical application, Trends Biotechnol. 30 (2012) 350–359. doi:10.1016/J.TIBTECH.2012.03.003.

[34] C. McKee, G.R. Chaudhry, Advances and challenges in stem cell culture, Colloids Surfaces B Biointerfaces. 159 (2017) 62–77. doi:10.1016/J.COLSURFB.2017.07.051.

[35] A.K. Gaharwar, S.M. Mihaila, A. Swami, A. Patel, S. Sant, R.L. Reis, A.P. Marques, M.E. Gomes, A. Khademhosseini, Bioactive silicate nanoplatelets for osteogenic differentiation of human mesenchymal stem cells, Adv. Mater. 25 (2013) 3329–3336. doi:10.1002/adma.201300584.

[36] M. Westhrin, M. Xie, M.Ø. Olderøy, P. Sikorski, B.L. Strand, T. Standal, Osteogenic Differentiation of Human Mesenchymal Stem Cells in Mineralized Alginate Matrices, PLoS One. 10 (2015) e0120374. doi:10.1371/journal.pone.0120374.

[37] S.X. Hsiong, T. Boontheekul, N. Huebsch, D.J. Mooney, Cyclic Arginine-Glycine-Aspartate Peptides Enhance Three-Dimensional Stem Cell Osteogenic Differentiation, Tissue Eng. Part A. 15 (2009) 263–272. doi:10.1089/ten.tea.2007.0411.

[38] A.D. Augst, H.J. Kong, D.J. Mooney, Alginate Hydrogels as Biomaterials, Macromol. Biosci. 6 (2006) 623–633. doi:10.1002/mabi.200600069.

[39] K.Y. Lee, D.J. Mooney, Alginate: Properties and biomedical applications, Prog. Polym. Sci. 37 (2012) 106–126. doi:10.1016/J.PROGPOLYMSCI.2011.06.003.

[40] J.A. Rowley, G. Madlambayan, D.J. Mooney, Alginate hydrogels as synthetic extracellular matrix materials, Biomaterials. 20 (1999) 45–53. doi:10.1016/s0142-9612(98)00107-0.

[41] T. Andersen, P. Auk-emblem, M. Dornish, 3D Cell Culture in Alginate Hydrogels, Microarrays. 4 (2015) 133–161. doi:10.3390/microarrays4020133.

[42] A. Khademhosseini, R. Langer, Microengineered hydrogels for tissue engineering, Biomaterials. 28 (2007) 5087–5092. doi:10.1016/j.biomaterials.2007.07.021.

[43] Y.-H. Tsou, J. Khoneisser, P.-C. Huang, X. Xu, Hydrogel as a bioactive material to regulate stem cell fate, Bioact. Mater. 1 (2016) 39–55. doi:10.1016/j.bioactmat.2016.05.001.

[44] M. Mehrasa, M.A. Asadollahi, B. Nasri-Nasrabadi, K. Ghaedi, H. Salehi, A. Dolatshahi-Pirouz, A. Arpanaei, Incorporation of mesoporous silica nanoparticles into random electrospun PLGA and PLGA/gelatin nanofibrous scaffolds enhances mechanical and cell proliferation properties, Mater. Sci. Eng. C. 66 (2016) 25–32. doi:10.1016/j.msec.2016.04.031.

[45] M. Mehrasa, M.A. Asadollahi, K. Ghaedi, H. Salehi, A. Arpanaei, Electrospun aligned PLGA and PLGA/gelatin nanofibers embedded with silica nanoparticles for tissue engineering, Int. J. Biol. Macromol. 79 (2015) 687–695. doi:10.1016/j.ijbiomac.2015.05.050.

[46] M.K. Jaiswal, J.R. Xavier, J.K. Carrow, P. Desai, D. Alge, A.K. Gaharwar, J. Accepted, Mechanically Stiff Nanocomposite Hydrogels at Ultralow Nanoparticle Content, ACS Nano. 10 (2016) 246–256. doi:10.1021/acsnano.5b03918.

[47] C.K. Balavigneswaran, S.K. Mahto, A.K. Mahanta, R. Singh, M.R. Vijayakumar, B. Ray, N. Misra, Cell proliferation influenced by matrix compliance of gelatin grafted poly(D,L-Lactide) three dimensional scaffolds, Colloids Surfaces B Biointerfaces. 166 (2018) 170–178. doi:10.1016/j.colsurfb.2018.03.014.

[48] R. Yao, R. Zhang, J. Luan, F. Lin, Alginate and alginate/gelatin microspheres for human adipose-derived stem cell encapsulation and differentiation, Biofabrication. 4 (2012) 025007. doi:10.1088/1758-5082/4/2/025007.

[49] Y. Zheng, X. You, L. Chen, J. Huang, L. Wang, J. Wu, S. Guan, Biotherapeutic Nanoparticles of Poly(Ferulic Acid) Delivering Doxorubicin for Cancer Therapy, J. Biomed. Nanotechnol. 15 (2019) 1734–1743. doi:10.1166/jbn.2019.2798.

[50] X. Zhou, W. Feng, K. Qiu, L. Chen, W. Wang, W. Nie, X. Mo, C. He, BMP-2 Derived Peptide and Dexamethasone Incorporated Mesoporous Silica Nanoparticles for Enhanced Osteogenic Differentiation of Bone Mesenchymal Stem Cells., ACS Appl. Mater. Interfaces. 7 (2015) 15777–89. doi:10.1021/acsami.5b02636.

[51] N. Taebnia, D. Morshedi, S. Yaghmaei, F. Aliakbari, F. Rahimi, A. Arpanaei, Curcumin-Loaded Amine-Functionalized Mesoporous Silica Nanoparticles Inhibit α-Synuclein Fibrillation and Reduce Its Cytotoxicity-Associated Effects, Langmuir. 32 (2016) 13394–13402.

doi:10.1021/acs.langmuir.6b02935.

[52] L. Rashidi, F. Ganji, E. Vasheghani-Farahani, Fluorescein isothiocyanate-dyed mesoporous silica nanoparticles for tracking antioxidant delivery, IET Nanobiotechnology. 11 (2017) 454–462. doi:10.1049/iet-nbt.2016.0120.

[53] F. Behzadi, S. Darouie, S.M. Alavi, P. Shariati, G. Singh, A. Dolatshahi-Pirouz, A. Arpanaei, Stability and Antimicrobial Activity of Nisin-Loaded Mesoporous Silica Nanoparticles: A Game-Changer in the War against Maleficent Microbes, J. Agric. Food Chem. 66 (2018) 4233–4243. doi:10.1021/acs.jafc.7b05492.

[54] K.J. Livak, T.D. Schmittgen, Analysis of Relative Gene Expression Data Using Real-Time Quantitative PCR and the 2−ΔΔCT Method, Methods. 25 (2001) 402–408. doi:10.1006/meth.2001.1262.

[55] Y.M. Mohan, T. Premkumar, K. Lee, K.E. Geckeler, Fabrication of Silver Nanoparticles in Hydrogel Networks, Macromol. Rapid Commun. 27 (2006) 1346–1354. doi:10.1002/marc.200600297.

[56] O. Veiseh, J.C. Doloff, M. Ma, A.J. Vegas, H.H. Tam, A.R. Bader, J. Li, E. Langan, J. Wyckoff, W.S. Loo, S. Jhunjhunwala, A. Chiu, S. Siebert, K. Tang, J. Hollister-Lock, S. Aresta-Dasilva, M. Bochenek, J. Mendoza-Elias, Y. Wang, M. Qi, D.M. Lavin, M. Chen, N. Dholakia, R. Thakrar, I. Lacík, G.C. Weir, J. Oberholzer, D.L. Greiner, R. Langer, D.G. Anderson, Size- and shape-dependent foreign body immune response to materials implanted in rodents and non-human primates, Nat. Mater. 14 (2015) 643–651. doi:10.1038/nmat4290.

[57] S. Farris, J. Song, Q. Huang, Alternative Reaction Mechanism for the Cross-Linking of Gelatin with Glutaraldehyde, J. Agric. Food Chem. 58 (2010) 998–1003. doi:10.1021/jf9031603.

[58] A.J. Kuijpers, G.H. Engbers, J. Krijgsveld, S.A. Zaat, J. Dankert, J. Feijen, Cross-linking and characterisation of gelatin matrices for biomedical applications., J. Biomater. Sci. Polym. Ed. 11 (2000) 225–43. doi:10.1163/156856200743670.

[59] H.-I. Chang, Y. Wang, Cell Responses to Surface and Architecture of Tissue Engineering Scaffolds, in: Regen. Med. Tissue Eng. - Cells Biomater., InTech, 2011. doi:10.5772/21983.

[60] J.H. Lee, H.W. Jung, I.K. Kang, H.B. Lee, Cell behaviour on polymer surfaces with different functional groups., Biomaterials. 15 (1994) 705–11. doi:10.1016/0142-9612(94)90169-4.

[61] U. Riekstina, I. Cakstina, V. Parfejevs, M. Hoogduijn, G. Jankovskis, I. Muiznieks, R. Muceniece, J. Ancans, Embryonic Stem Cell Marker Expression Pattern in Human Mesenchymal Stem Cells Derived from Bone Marrow, Adipose Tissue, Heart and Dermis, Stem Cell Rev. Reports. 5 (2009) 378–386. doi:10.1007/s12015-009-9094-9.

[62] J.R. Xavier, T. Thakur, P. Desai, M.K. Jaiswal, N. Sears, E. Cosgriff-Hernandez, R. Kaunas, A.K. Gaharwar, Bioactive Nanoengineered Hydrogels for Bone Tissue Engineering: A Growth-Factor-Free Approach, ACS Nano. 9 (2015) 3109–3118. doi:10.1021/nn507488s.

[63] A. Paul, V. Manoharan, D. Krafft, A. Assmann, J.A. Uquillas, S.R. Shin, A. Hasan, M.A. Hussain, A. Memic, A.K. Gaharwar, A. Khademhosseini, Nanoengineered biomimetic hydrogels for guiding human stem cell osteogenesis in three dimensional microenvironments, J. Mater. Chem. B. 4 (2016) 3544–3554. doi:10.1039/C5TB02745D.

[64] N. Ahmed, J. Iu, C.E. Brown, D.W. Taylor, R.A. Kandel, Serum-and Growth-Factor-Free Three-Dimensional Culture System Supports Cartilage Tissue Formation by Promoting Collagen Synthesis via Sox9-Col2a1 Interaction, Tissue Eng. Part A. 20 (2014) 2224–2233. doi:10.1089/ten.tea.2013.0559.

[65] G.B. Schneider, A. English, M. Abraham, R. Zaharias, C. Stanford, J. Keller, The effect of hydrogel charge density on cell attachment, Biomaterials. 25 (2004) 3023–3028. doi:10.1016/J.BIOMATERIALS.2003.09.084.

[66] M. Dadsetan, M. Pumberger, M.E. Casper, K. Shogren, M. Giuliani, T. Ruesink, T.E. Hefferan, B.L. Currier, M.J. Yaszemski, The effects of fixed electrical charge on chondrocyte behavior, Acta Biomater. 7 (2011) 2080–2090. doi:10.1016/J.ACTBIO.2011.01.012.

[67] A. Higuchi, Q.-D. Ling, Y. Chang, S.-T. Hsu, A. Umezawa, Physical Cues of Biomaterials Guide Stem Cell Differentiation Fate, Chem. Rev. 113 (2013) 3297–3328. doi:10.1021/cr300426x.

[68] L. Ding, X. Zhu, Y. Wang, B. Shi, X. Ling, H. Chen, W. Nan, A. Barrett, Z. Guo, W. Tao, J. Wu, X. Shi, Intracellular Fate of Nanoparticles with Polydopamine Surface Engineering and a Novel Strategy for Exocytosis-Inhibiting, Lysosome Impairment-Based Cancer Therapy, Nano Lett. 17 (2017) 6790–6801. doi:10.1021/acs.nanolett.7b03021.

[69] M.-C. Hofmann, Stem Cells and Nanomaterials, in: Adv. Exp. Med. Biol., 2014: pp. 255–275. doi:10.1007/978-94-017-8739-0_13.

## Highlights

- Mesoporous silica nanoparticles were used to reinforced polysaccharide-based hydrogels
- Nanoparticles surface chemistry and concentration highly affect stem cells fate and homogeneity in hydrogel-based 3D scaffolds
- Encapsulated human adipose-derived stem cells maintain their stemness when cultured in alginate/gelatin hydrogel beads incorporated with amine-functionalized silica nanoparticles

## Declaration of competing interest:

We declare that no conflict of interest exists.